II

Publication II

T. Laaksonen, P. Ahonen, C. Johans and K. Kontturi, Stability and Electrostatics of Mercaptoundecanoic Acid Capped Gold Nanoparticles with Varying Counter-Ion Sizes, *ChemPhysChem*, 2006, **7**(10), 2143-2149.

Article

Stability and electrostatics of mercaptoundecanoic acid capped gold nanoparticles with varying counter-ion sizes

M.Sc. Timo Laaksonen[a], M.Sc. Päivi Ahonen[a], D.Sc. Christoffer Johans[a] and Prof. Kyösti Kontturi*[a]

[a] *Laboratory of Physical Chemistry and Electrochemistry, Helsinki University of Technology, P.O. Box 6100, FIN-02015 HUT, Finland.*

Fax: (+358)-9-451 2580

E-mail: kontturi@cc.hut.fi

Increased stability with larger counter-ions. The solubility of charged nanoparticles can be critically dependent on pH and counter-ion size. Here, greatly enhanced stability for mercaptoundecanoic acid capped gold particles was observed with bulky quaternary ammonium hydroxides. This was shown to be linked to a strongly bound ion layer at the particle surface.

Colloids

Electric double-layer

Electrochemistry

Zeta-potential

The solubility of charged nanoparticles can be critically dependent on pH. However, the concentration range available with bases such as NaOH is quite narrow since the particles precipitate due to the compression of the electric double layer when the ionic strength is increased. The stability of MUA capped Au-nanoparticles was studied using hydroxides to set the pH, while using bases with cations of different sizes. The counter-ions used were sodium (Na^+), tetramethylammonium (TMA^+), tetraethylammonium (TEA^+) and tetrabutylammonium (TBA^+). The particles precipitated in the 70 - 90 mM range with Na^+ as the counter-ion, however, with quaternary ammonium hydroxides the particles were stable even in concentrations exceeding 1 M. The change in solubility was linked to a strongly adsorbed layer on the surface of the ligand shell of the nanoparticles. The increased concentration range obtained with TEAOH was further used to facilitate thiol exchange to an extent, which would have been impossible to do in NaOH solutions.

1. Introduction

Water-soluble metallic nanoparticles have been the subject of continued interest and many prospective applications in biosciences have recently been demonstrated.[1-4] They can be used for example in bio-electronic devices,[2] as label molecules[2] and in targeted drug delivery[3]. While it is quite easy to make stable monolayer protected nanoparticles soluble in organic solvents by using standard procedures such as the Brust-Schiffrin method,[5] isolable, stable water-soluble particles are more difficult to make. These are commonly charge-stabilized particles that are protected by carboxylic acid or amine terminated ligands. Citrate stabilized gold particles can be prepared using the classic Turkevich method where citrate is used as a simultaneous capping and reducing agent.[6] However, the particles cannot be isolated from solution without irreversible aggregation, which restricts their use for applications. In contrast, the Kimura method with mercaptosuccinic acid or mercaptoundecanoic acid as the capping agent and sodium borohydride as the reductant[7-10] generates thiol stabilized particles with a carboxylic acid functionality. These particles can be repeatedly isolated and redispersed in aqueous solution. As the solubility and stability of these thiol stabilized particles is closely linked to the double layer structure and pH of the system,[10-12] full characterization is essential for their successful utilization in future applications.

At low pH, carboxylic acid-stabilized nanoparticles agglomerate due to protonation and hydrogen bonding,[11] rendering them soluble only in basic conditions. At high pH, the carboxylic acid groups deprotonate and stabilize the particle dispersion through electrostatic repulsion. Overlap of the electrical double layers surrounding the particles prevents them from approaching each other and agglomerating by attractive van der Waals forces. The double layer is contracted and surface potential decreased with increasing salt concentration and therefore the particles coagulate when the ionic strength exceeds a limit known as the critical coagulation concentration (c.c.c.). This limit

depends strongly on the charge of the counter-ion (Schulze-Hardy rule[13]) and only to a smaller extent on the structure and size of the ion. Typically this limit is low, between 50 – 100 mM for monovalent counter-ions and much lower for multivalent counter-ions.[13] A common theory for describing the stability of colloidal systems of this type is the Derjaguin-Landau-Verwey-Overbeek (DLVO) theory,[1, 13] which works qualitatively well for most systems, but needs modifications at very small length scales.[14, 15]

In most reports, the nanoparticle solution pH is fixed with NaOH.[8, 9, 11, 12] However, it would be interesting to consider the effect of counter-ion size as this will alter the distance of closest approach and change the double layer structure. This change should be noted when calculating the surface potential and potential distribution around a nanoparticle. The effect of a probable adsorbed layer can easily be incorporated with previous calculations of the double layer structure[16] by taking the charge separation between carboxylic acid groups and their counter-ions into account. The concept of ion size in DLVO theory was already proposed in 1972 by Frens and Overbeek, who estimated that large counter-ions could enhance the stability of colloids by increasing the distance of closest approach for two colloids to twice the diameter of the counter-ions.[17]

In the current work, mercaptoundecanoic acid (MUA) was chosen as the capping agent to simplify the ligand shell structure. MUA has only one pKa value and provides good stability against aggregation of the metallic cores.[7] The effect of different counter-ions (Na^+, TMA^+, TEA^+ and TBA^+) on the stability of the nanoparticles was studied by light scattering and zeta potential measurements. A model taking counter-ion size into account was used to explain differences noted in particle solubility and zeta potential for each ion. As a demonstration of the effect of counter-ion size on the particle electrokinetic properties, we show that the particle double layer structure and surface potential can be used to control the extent of ligand exchange reactions where the charged thiolate ligand on the particle surface is replaced with an incoming ligand from the

solution.[18] This was studied by exchanging MUA to a bivalent mercaptosuccinic acid (MSA). At low ionic strength the strong electrostatic repulsion between the negatively charged MUA and MSA should cause the surface concentration of MSA to drop to nearly zero, thus efficiently blocking the thiol exchange reaction. Increasing the solution ionic strength decreases the absolute value of surface potential and therefore the reaction should be facilitated with increased salt concentration.

2. Results and Discussion

2.1. Electric double-layer model

The electrical double layer around a spherical particle can be solved using the Poisson-Boltzmann equation:

$$\begin{cases} \nabla^2\psi = -\dfrac{\rho}{\varepsilon} = \kappa^2 \sinh\left(\dfrac{F}{RT}\psi\right) \\ \dfrac{\partial}{\partial r}\psi\Big|_{r=a} = \dfrac{-\sigma}{\varepsilon_r\varepsilon_0} = \dfrac{-ze}{4\pi\varepsilon_r\varepsilon_0 a^2} \end{cases} \quad (1)$$

where ψ is the potential, ρ is the charge density, σ is the charge density at the surface of the particle, ε is the dielectric constant, z is the number of charges at the surface, e is the elementary charge and a is the size of the particle *i.e.* the sum of the radius of the particle core (r_c) and the thickness of the ligand shell (l). κ, the inverse of the Debye length, is defined as

$$\kappa = \sqrt{\frac{2F^2 c_e}{\varepsilon_r\varepsilon_0 RT}} \quad (2)$$

The problem with the Poisson-Boltzmann equation for the spherical case with low κa, is the non-linearity which means that the equations usually have to be solved numerically. The calculations can be made considerably simpler by applying the analytical approximations developed by Ohshima *et. al.* for the relation of charge density to surface potential and the potential distribution around the particle:[16]

$$\sigma = \left(8c_e\varepsilon_r\varepsilon_0 RT\right)^{1/2}\left[1+\frac{1}{\kappa a}\frac{2}{\cosh^2\left(f\psi^0/2\right)}+\frac{8}{(\kappa a)^2}\frac{\ln\left[\cosh\left(f\psi^0/4\right)\right]}{\sinh^2\left(f\psi^0/4\right)}\right]^{1/2} \quad (3)$$

$$\psi(r) = \frac{2kT}{e}\ln\left[\frac{(1+Bs)\left[1+Bs/(2\kappa a+1)\right]}{(1-Bs)\left[1-Bs/(2\kappa a+1)\right]}\right] \quad (4)$$

where $f = F/RT$, ψ^0 is the surface potential and

$$s = \frac{a}{r}\exp\left[-\kappa(r-a)\right] \quad (5)$$

$$B = \frac{\left[1+\kappa a/(\kappa a+1)\right]\tanh\left(e\psi^0/4kT\right)}{1+\left\{1-\left[(2\kappa a+1)/(\kappa a+1)^2\right]\tanh^2\left(e\psi^0/4kT\right)\right\}^{1/2}} \quad (6)$$

These equations are valid to within 5% when $\kappa a > 0.1$.[16]

Here, we use a Stern-Gouy-Chapman type model adapted from Valleau and Torrie[19] to describe the structure of the double layer. In this model, the finite size of the counter-ions is taken into account by assuming that there is a layer of zero charge density due to the distance of closest approach next to the particle surface as presented in Figure 1. Thus $\rho = 0$ in area I), and the Poisson-Boltzmann equation is applied in area II. Also illustrated in Figure 1 is the slipping plane, which is defined so that all ions inside move with the particle when it is subjected to an external electric field. The potential at that point is called the zeta potential, ζ, and is an indirectly measurable quantity. The location of the slipping plane is a model dependent quantity, which depends on the ionic strength and the type of the ions in the system.

The solution in area I) is trivial:

$$\nabla^2\psi^I = 0 \quad (7)$$

$$\psi^I(r) = \frac{ze}{4\pi\varepsilon_r\varepsilon_0}\frac{1}{r}+b \quad (8)$$

where b is an integration constant that can be determined from the continuity of electric displacement between area I and II. Superscript I refers to area I. In area II, the Ohshima model is applied. Solving eq (1) –(8) with realistic parameters leads to potential profiles

such as shown in Figure 2. In Figure 3, the same calculations are done with varying counter-ion sizes. Even though surface potentials are different with varying thickness of the adsorbed layer, potentials at the onset of area II are quite close to each other.

2.2. DLVO-theory

Next we consider the colloidal stability of the system. Again we take a simple approach and assume that we can get at least qualitative information from the standard DLVO-theory. There are a number of ways to calculate the repulsion and attraction for colloidal systems. Here we take the same approach as recently used by Kim *et al.*[20] and use the linear superposition method for electrostatic repulsion[21] and van der Waals forces as the attractive force[1]. The sum of these will be the total interaction energy between two particles. The model assumes that electrostatic potentials of two particles overlap and can be superposed. Furthermore, it is assumed that the Gouy-Chapman model applies, and hence does not include the Stern layer. This simplification is small compared to the assumed superposing of the electrostatic potentials. The repulsive force is then the integral of the net stress tensor over a particle surface and the repulsive potential can be written as follows:

$$V_{\text{rep}} = 4\pi a^2 \left(\psi^0\right)^2 \left(\frac{RT}{F}\right)^2 \frac{e^{-\kappa h}}{2a+h} \tag{9}$$

where h is the surface to surface separation and ψ^0 is the surface potential of the particle calculated by eq. (1) - (8). The attractive potential between two particles is:

$$V_{\text{attr}} = -\frac{A_H}{6}\left[\frac{2a^2}{h^2+4ah} + \frac{2a^2}{(h+2a)^2} + \ln\frac{h^2+4ah}{(h+2a)^2}\right] \tag{10}$$

where A_H is the Hamaker's constant that is taken to be around $110kT$ for the current case.[3]

2.3. Stability of nanoparticle solutions

TEM-measurements showed that the as-prepared particles were reasonably monodisperse. The mean diameter of the particles was 2.3 nm, which corresponds to around 90 ligands on the particle surface.[22] This was used as the number of charges *z* in the calculations. It is assumed that all ligands are dissociated, since an excess of strong base was used in all experiments. The as-prepared nanoparticles did not dissolve in water directly. To make a 10 mg/ml solution of particles, a hydroxide concentration of around 10 mM was needed. This could then be diluted by a factor of 100 times without any precipitation. The solubility is therefore not concentration dependent, but rather a weak acid – strong base reaction, where we need to have stoichometric amounts of hydroxide compared to mercaptoundacanoic acid to deprotonate the ligand shell. The choice of the counter-ion did not have any effect on the lower solubility limit.

The effect of counter-ion size was first seen when nanoparticles were coagulated by increasing the hydroxide concentration. All nanoparticles precipitated out of the solution when the NaOH concentration exceeded 90 mM. Precipitation was observed even at 70 mM NaOH given enough time. However, with TMAOH, TEAOH and TBAOH no upper solubility limit was reached in the concentration range studied here and the particles remained dispersed in solution even at 1 M salt concentrations. If sufficient NaOH was added to these solutions, it would induce precipitation indicating that quaternary ammonium ions and Na^+ have a competing interaction at the particle surface. Conversly, it was possible to add a high amount of TEAOH into NaOH solutions without causing precipitation regardless of the high ionic strength reached.

Zeta potential measurements (Figure 4) showed that with increasing counter-ion size, the value of the zeta potential shifted to less negative potentials. This follows from more efficient shielding of the negative surface charge. The magnitude of the zeta potential is commonly taken as a measure of colloidal stability. However, since the surface charge is the same for all cases and comparative concentrations were used for all

counter-ions, the increased stability observed with the quaternary ammonium hydroxides must be due to other reasons, i.e. the double layer structure. When determining the zeta potential, it is good to remember that the instrument used actually measures electrophoretic mobility and not the zeta potential. Here, we used the Hückel approximation to convert mobility to zeta potential. Even though better theories exist, such as the one by White *et. al*.[24] and the simpler analytical form by Ohshima,[25] it was calculated that the difference between these theories in the current case should fall below the experimental accuracy of 3 mV.

The location of the slipping plane was determined as the radius where the modeled potential equals the zeta potential determined from the experiment, and is shown in Figure 5 as a function of κa. The calculations revealed that the location of the slipping plane shifted further from the surface of the nanoparticles with increasing counter-ion size. A simple fit was made where the location of the slipping plane was assumed to follow a formula $\alpha\kappa^{-1}+\beta$, where the first part corresponds to the stretching of the double layer due to changes in ionic strength (Area II) and the second part is due to the size of the particle and Stern layer (Area I). The best fit was obtained with $\alpha \approx 1/5$ and $\beta \approx a + 2d_{\text{counter-ion}}$. As can be seen in Figure 5, this seems to fit the data quite well. The term $2d_{\text{counter-ion}}$ describes the thickness of the Stern layer. We believe that the reason that the thickness of the Stern layer is larger than the counter-ion size must arise from the hydration of the ions present. Even though the choice for the slipping plane is arbitrary, it has a physical meaning as well. For very high ionic strengths, the first term disappears and only the term for ions adsorbed in the Stern layer is left. The measurements thus indicate the formation of a steric barrier against aggregation, and confirm the applicability of the idea proposed by Frens and Overbeek[17] to MUA stabilized gold nanoparticles. When two particles approach each other, they probably can share the same

adsorbed layer, but cannot come closer than that. This is the distance of closest approach for two nanoparticles.

It is straightforward to calculate interaction energy between two particles using eq. (9) and (10). The results are given in Figure 6. If we take the distance of closest approach between to particles to be twice the diameter of the counter-ion, as justified by the electrostatically adsorbed Stern layer, it is clear that the efficient interaction energy for bigger counter-ions will never reach a minimum, since the strong drop in the interaction energy will begin inside the distance of closest approach for two particles. But for smaller ions, such as Na^+, there will always be an energy minimum that causes the aggregation of the nanoparticles.[17] Thus, a steric hindrance caused by the ions adsorbed in the Stern layer stabilizes the nanoparticles against aggregation in quaternary ammonium hydroxide solutions. Coupling the carboxylic acid groups of the ligand shell with large counter-ions can be used to make them stable even at high ionic strengths.

The particle size was also studied by dynamic light scattering (DLS). In the light scattering experiments fluctuations in the scattered light are measured and related to the diffusion of hard sphere particles through the Stokes-Einstein relation[1] and hence, provides a simple means to measure the hydrodynamic radii of a colloid. The hydrodynamic radius differs from the real radius because it is affected by the solvent structure surrounding the particles. A charged sphere drags a large amount of solvent molecules and ions bound in the double layer with it, and consequently, it has a larger diffusion coefficient than a non-charged sphere of the same size.

DLS can also be used to study agglomeration in solution, since the intensity of the scattered light depends on the radius of the scattering object to a power of six, and therefore the method is very sensitive to the formation of larger particle clusters. The measured radii ranged between 20 and 100 nm. These values are almost one order of magnitude larger than expected from the location of the slipping plane and the particle

size given by the TEM analysis. In the discussion below, it is assumed that this follows from the formation of soluble clusters of particles. These clusters may form and dissolve continuously with the thermal fluctuations. It is proposed that the reason that the hydrodynamic size obtained from the zeta potential measurements differ from that obtained from light scattering is due to the break up of the clusters in by the electric field present in the zeta potential measurements. Thus, the size of the clusters obtained from the intensity distribution is taken as a measure of the colloidal stability of the solution. It is also noted here that if the hydrodynamic diameter is evaluated from the number distribution instead of the intensity distribution, large clusters can be observed only for NaOH (figure not shown).

The size as a function of κa is presented in Figure 7. When the NaOH concentration is increased the average hydrodynamic radius increases as well. Higher ionic strength reduces the electrostatic repulsion between the particles, as expected based on the DVLO theory, and hence larger clusters tend to form. However, quaternary ammonium hydroxides induced an opposite trend. With increasing hydroxide concentration the hydrodynamic radius decreased, which is attributed to the stabilization of the particles resulting in the formation of smaller clusters. This was unexpected, as it suggests that the particles are actually stabilized by a higher salt concentration. Furthermore, the decrease is more prominent with larger quaternary ammonium counter-ion size (Table 1) verifying the role of the counter-ions as steric barriers.

2.4. Thiol-exchange studies

It is possible to take advantage of the increased concentration range available for bigger counter-ions. Normally, it would be very challenging to exchange mercaptoundecanoinc acid to mercaptosuccinic acid at the nanoparticle surface due to strong electrostatic repulsion. However, with quaternary ammonium salts, for example TEAOH, the barrier can easily be eliminated by using high salt concentrations. To test

this hypothesis, thiol exchange was done in two concentrations, 60 mM TEAOH and 860 mM TEAOH. Theoretically, this should lead to approximately 60 mV drop in the surface potential, certainly sufficient to influence the extent of thiol exchange. While, the lower concentration would be available in NaOH solutions without inducing aggregation, the latter is too high for all small counter-ions. In both cases, the MUA stabilized nanoparticles were mixed with an excess of mercaptosuccinic acid for 7 days, after which the particles were purified.

The hydrodynamic diameter and zeta potential of the particles subjected to thiol exchange were measured. The results are shown in Table 2. Because of changes in ligand shell structure and the uncertainty of the value of the surface charge density, this data can be used for qualitative purposes only. Nevertheless, from the large shift in zeta potential in the 860 mM case we can conclude that the thiol exchange reaction had proceeded further than in the 60 mM case where only a 4 mV drop in zeta potential is seen. The more negative zeta potential reflects the more negative surface potential resulting from higher charge density obtained by exchanging the bivalent ligand to a monovalent ligand. The surface potential should directly influence the extent of thiol exchange θ at equilibrium as shown by the following equations.

$$MSA^{2-} + \text{Au-MUA}^{-} \leftrightarrow MUA^{-} + \text{Au-MSA}^{2-} \tag{11}$$

$$\frac{d\Gamma_{\mathrm{MSA}}}{dt} = k_f c^{\mathrm{s}}_{\mathrm{MSA}} \Gamma_{\mathrm{MUA}} - k_b c^{\mathrm{s}}_{\mathrm{MUA}} \Gamma_{\mathrm{MSA}} \tag{12}$$

where Γ_{i} is the surface concentration of each species, k_f and k_b are the rate constants for forward and backward reaction and $c^{\mathrm{s}}_{\mathrm{i}}$ is the concentration of each species near the surface of the particle defined by the Gouy-Chapman theory.

$$c^{\mathrm{s}}_{\mathrm{i}} = c^{\mathrm{bulk}}_{\mathrm{i}} \exp\left(-\frac{zF}{RT} \psi^{0} \right) \tag{13}$$

The extent of thiol exchange is defined as a ratio of the surface concentration of MSA to the surface concentration of all available surface locations.

$$\theta = \frac{\Gamma_{\mathrm{MSA}}}{\Gamma_{\mathrm{TOT}}} \tag{14}$$

$$\frac{d\theta}{dt} = k_f c_{MSA}^{bulk} \exp\left(\frac{2F}{RT}\psi^0\right)(1-\theta) - k_b c_{MUA}^{bulk} \exp\left(\frac{F}{RT}\psi^0\right)\theta \tag{15}$$

The equilibrium constant is defined as follows

$$K = \frac{k_f}{k_b} = \frac{\theta_{eq}}{(1-\theta_{eq})} \exp\left(-\frac{F}{RT}\psi^{0,eq}\right) \frac{c_{\mathrm{MSA}}^{\mathrm{bulk,eq}}}{c_{\mathrm{MUA}}^{\mathrm{bulk,eq}}} \tag{16}$$

From eq. (16) it follows directly that the possible 60 mV drop in the surface potential with increased salt concentration could lead to up to 6 times larger values of θ_{eq}, depending on the value of K. The equilibrium bulk thiol concentrations and the surface potential changes with the extent of reaction, and hence, the reaction equilibrium will shift. Nevertheless, a large change was observed, confirming the facilitating effect of salt concentration to thiol exchange.

3. Conclusions

The stability of basic aqueous solutions of mercaptoundecanoic acid (MUA) capped Au-nanoparticles was studied by varying the counter-ions of the hydroxides. A significant difference was noted with quaternary ammonium ions in comparison to sodium, as these ions did not induce particle coagulation even at very high concentrations. To explain this effect, electrostatics and double layer structure surrounding the nanoparticles were considered using a Stern-Gouy-Chapman type double layer structure and DLVO theory. The anomalous effect was linked to an adsorbed layer of counter-ions on the surface of the ligand shell of the nanoparticles, which acts as a steric barrier and increases the distance of closest approach for two nanoparticles. It was possible to use the higher salt concentrations available with the quaternary ammonium

counter-ions to facilitate ligand exchange of MUA to MSA. The reaction was shown to proceed much further in 860 mM TEAOH than in 60 mM TEAOH. The negative surface potential, which at lower salt concentrations would decrease the concentration of bivalent MSA on the surface of the nanoparticle, is made less negative in high ionic strength solutions allowing the thiol exchange to proceed. It appears that the choice of the electrolyte should be carefully considered when using this type of nanoparticles in aqueous environments. An easy modification of the system gives a greatly enhanced stability and even allows surface reactions that would otherwise not proceed. This should be taken into account especially in future bioapplications and in situations where one would rather have a single nanoparticle interaction instead of clusters of electrostatically bound nanoparticles.

Experimental Section

Chemicals used in the experiments: Tetrachloroaurate trihydrate ($HAuCl_4$, 99.9%, Sigma-Aldrich), mercaptoundecanoic acid (95%, Aldrich), mercaptosuccinic acid (97%, Aldrich), sodium borohydride ($NaBH_4$, Merck), methanol (p.a., Merck), sodium hydroxide (1 M solution, Merck), hydrochloric acid (1 M solution, Merck), tetramethylammonium hydroxide (1 M solution in water, Sigma-Aldrich), tetraethylammonium hydroxide (40 w-% solution in water, Sigma-Aldrich) were used as received. Tetrabutylammonium hydroxide (1 M solution in water, Sigma-Aldrich) was heated in a warm water bath to ensure full dissolution before use. All solutions were prepared with MQ® treated water.

Dynamic light scattering and zeta potential measurements were performed using a Zetasizer Nano ZS (Malvern Instruments). A 4 mW 633 nm He-Ne laser was used as the light source and the scattered light was measured at 173 degrees to prevent multiple scattering. The data was analyzed using standard procedures provided with the instrument software. The size distribution measurements were carried out in disposable plastic

cuvettes and zeta potentials were measured in disposable folded capillary cuvettes (Malvern Instruments). The Zeta potential was derived from the measured mobility data with the Hückel equation. The ionic strength of the samples was set by adding appropriate hydroxide to the nanoparticle solutions. It must be noted that zeta potential could not be reliably measured at high salt concentrations due to instrumental limitations. Also, a certain amount of base was always needed to keep the particles soluble. This results in a limit for dilution, since low particle concentrations are problematic for light scattering measurements. The Zeta potential measurements could be reliably performed at hydroxide concentrations from 0.5 mM to 50 mM. The concentration window was even narrower (1 - 10 mM) for TBAOH, which proved to be the most difficult to measure.

The nanoparticle size distribution was estimated with transmission electron microscopy. Measurements were performed on a Tecnai 12 instrument operating at a 120 kV accelerating voltage. The samples were prepared by placing a 6 µl drop of nanoparticles in water on formvar/carbon-coated copper grids (Electron Microscopy Sciences). The grids were dried in air overnight before measurement. Size analysis was done using the ImageJ software. UV-vis spectra were measured on a Cary 50 instrument (Varian) in disposable plastic cuvettes. Samples were diluted with fresh MQ® water prior to measurement.

The synthesis of gold nanoparticles followed closely the procedure of Kimura *et. al*.[10] Briefly, $HAuCl_4$ (410 mg) was dissolved in water (6 ml) and mixed with a methanol solution (200 ml) of mercaptoundecanoic acid (650 mg). A freshly prepared solution of $NaBH_4$ (380 mg in 20 ml water) was added dropwise under vigorous stirring in an ice bath to reduce the gold salt. The resulting dark-brown solution was stirred for an additional hour after which the reaction was complete. The nanoparticles were allowed to sediment to the bottom of the flask and were collected by decantation and centrifugation.

The particles were washed by dispersing them in 80% methanol and removing the solvent by centrifugation. This was repeated four times to remove impurities and byproducts. During the second washing, a drop of 1 M HCl was added to the test tubes to ensure that Na^+ ions were displaced from the mercaptoundecanoic acid groups. In the final step, the particles were washed with pure methanol. The particle mass was then dried in a vacuum overnight and dissolved in water at given hydroxide concentrations and weight ratios.

In the thiol exchange studies, mercaptoundecanoic acid on the surface of the nanoparticles was exchanged to mercaptosuccinic acid. This was performed at two different TEAOH concentrations: 60 mM and 860 mM. In both cases, 2 mg/ml of nanoparticles and 20 mM mercaptosuccinic acid were used. The reaction was allowed to proceed for 7 days before the solvent was removed using centrifugal filtration units (Microsep 30k Omega, Pall Life Sciences). The residue was redissolved in water and a drop of 1 M HCl was added to completely precipitate the particles. The solutions were further purified by repeating the filtration-redissolution cycle three times. The pH of the filtered water was neutral. Finally, TEAOH concentration of all samples was set to 5 mM in order to make their subsequent zeta potential measurements comparable to each other.

Acknowledgements

The authors would like to thank Dr. Bernadette Quinn for helpful comments and proof reading of the article.

[1] R. Vold, M. Vold, *Colloid and Interface Chemistry*, Addison-Wesley Publishing Company, Inc., Massachusetts, **1983**.

[2] C. M. Niemeyer, C. A. Mirkin, *Nanobiotechnology*, Wiley-VCH, Weinheim, **2004**.

[3] W. R. Glomm, *J. Dispersion Sci. Technol.* **2005**, 26, 389-414.

[4] S. K. Teresa Pellegrino, Tim Liedl, Almudena Muñoz Javier, Liberato Manna, Wolfgang J Parak, *Small* **2005**, *1*, 48-63.

[5] M. Brust, M. Walker, D. Bethell, D. J. Schiffrin, R. Whyman, *J. Chem. Soc., Chem. Commun.* **1994**, 801-802.

[6] B. V. Enustun, J. Turkevich, *J. Am. Chem. Soc.* **1963**, *85*, 3317-3328.

[7] S.-Y. Lin, Y.-T. Tsai, C.-C. Chen, C.-M. Lin, C.-h. Chen, *J. Phys. Chem. B* **2004**, *108*, 2134-2139.

[8] C. S. Weisbecker, M. V. Merritt, G. M. Whitesides, *Langmuir* **1996**, *12*, 3763-3772.

[9] K. Aslan, V. H. Perez-Luna, *Langmuir* **2002**, *18*, 6059-6065.

[10] S. Chen, K. Kimura, *Langmuir* **1999**, *15*, 1075-1082.

[11] C.-H. Su, P.-L. Wu, C.-S. Yeh, *Bull. Chem. Soc. Jpn.* **2004**, *77*, 189-193.

[12] K. Kimura, S. Takashima, H. Ohshima, *J. Phys. Chem. B* **2002**, *106*, 7260-7266.

[13] J. O. M. Bockris, B. E. Conway, E. Yeager, *Comprehensive Treatise of Electrochemitry. Volume 1; The Double Layer,* 2nd ed., Plenum Press, New York, **1984**.

[14] A. B. Glendinning, W. B. Russel, *J. Colloid Interface Sci.* **1983**, *93*, 95-104.

[15] J. D. Love, *J. Chem. Soc. Faraday Trans. 2* **1977**, *73*, 669-688.

[16] H. Ohshima, K. Furusawa, *Electrical phenomena at interfaces: Fundamentals, measurements and applications*, Markcel Dekker, New York, **1998**.

[17] G. Frens, J. T. G. Overbeek, *J. Colloid Interface Sci.* **1972**, *38*, 376-387.

[18] M. J. Hostetler, A. C. Templeton, R. W. Murray, *Langmuir* **1999**, *15*, 3782-3789.

[19] J. P. Valleau, G. M. Torrie, *J. Chem. Phys.* **1982**, *76*, 4623-4630.

[20] T. Kim, K. Lee, M.-S. Gong, S.-W. Joo, *Langmuir* **2005**, *21*, 9524-9528.

[21] P. Warszynski, Z. Adamczyk, *J. Colloid Interface Sci.* **1997**, *187*, 283-295.

[22] M. J. Hostetler, J. E. Wingate, C.-J. Zhong, J. E. Harris, R. W. Vachet, M. R. Clark, J. D. Londono, S. J. Green, J. J. Stokes, G. D. Wignall, G. L. Glish, M. D. Porter, N. D. Evans, R. W. Murray, *Langmuir* **1998**, *14*, 17-30.

[23] B. E. Conway, *Ionic Hydration in Chemistry and Biophysics*, Elsevier Scientific Publishing Company, Amsterdam, **1981**.

[24] R. W. O'Brien, L. R. White, *J. Chem. Soc. Faraday Trans. 2* **1978**, *74*, 1607-1626.

[25] H. Ohshima, *J. Colloid Interface Sci.* **2001**, *239*, 587-590.

Received: ((will be filled in by the editorial staff))

Published online on ((will be filled in by the editorial staff))

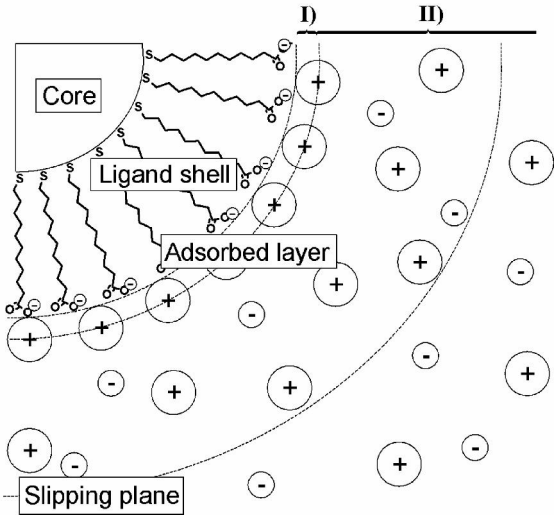

Figure 1. Schematic picture of the double layer structure surrounding a nanoparticle with charged ligands on its surface. The solvent molecules are not explicitly considered in this model.

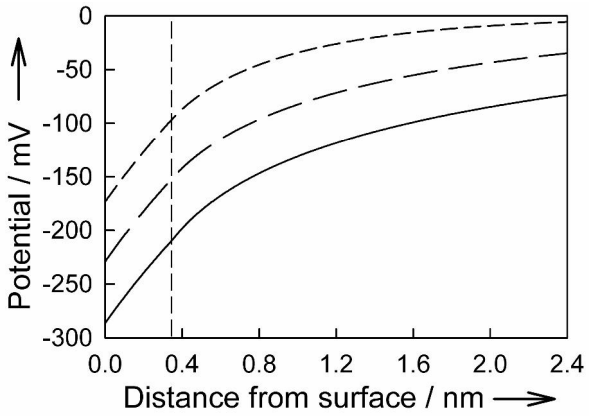

Figure 2. Potential profiles calculated for a MUA coated nanoparticle with r_c = 1.15 nm, l = 1.4 nm and z = 90, in TEAOH solutions with concentrations of 1 mM (solid), 10 mM (long dash) and 100 mM (short dash). Vertical line marks the boundary between areas I and II.

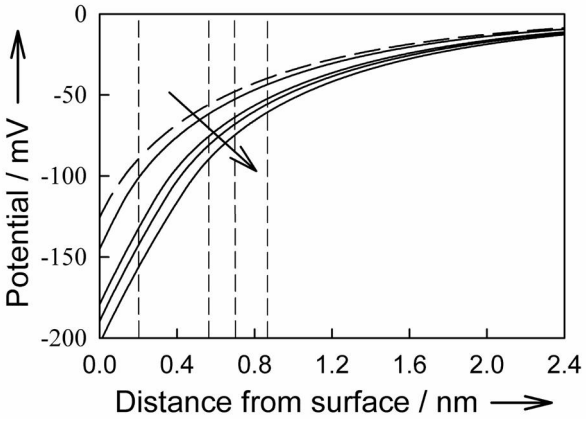

Figure 3. Potential profiles calculated for a MUA coated nanoparticle with r_c = 1.15 nm, l = 1.4 nm and z = 90 in 50 mM salt concentration with increasing counter-ion size as indicated by the arrow. Dashed line corresponds to a model without an adsorbed layer and other lines correspond to Na^+, TMA^+, TEA^+ and TBA^+ as counter-ions. Vertical lines mark the sizes of each counter-ion.

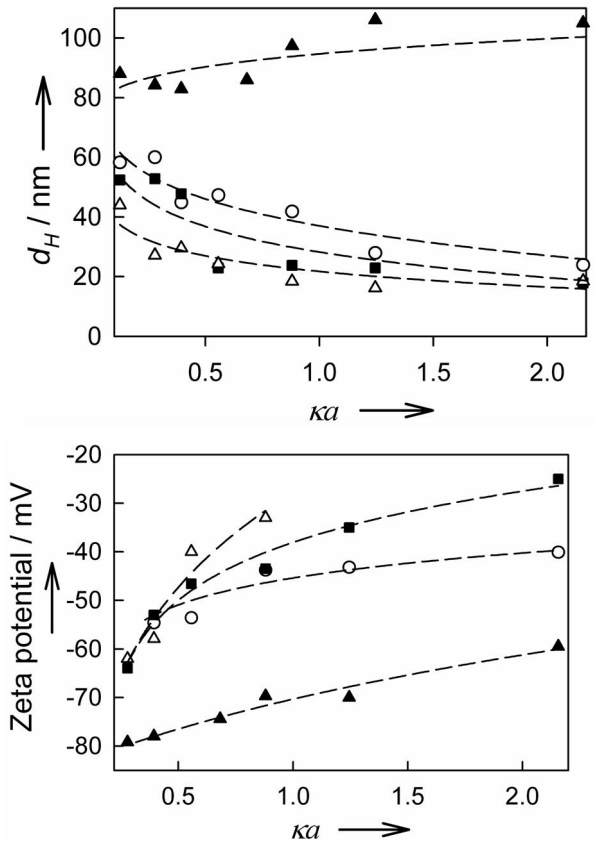

Figure 4. Hydrodynamic diameter (a) and zeta potential (b) of MUA-capped nanoparticles with varying counter-ions at different salt concentrations: Na^+ (solid triangle), TMA^+ (circle), TEA^+ (square) and TBA^+ (triangle). Dashed lines are added as guides to the eye.

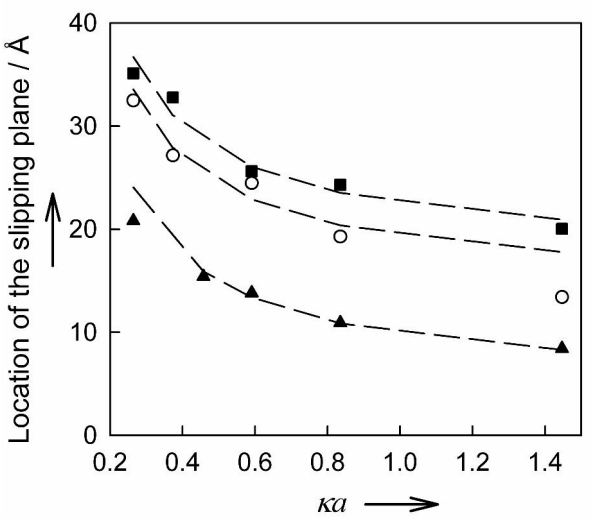

Figure 5. Location of the slipping plane as a distance from the surface of the ligand shell at different concentrations with varying counter-ions: Na^+ (triangle), TMA^+ (circle) and TEA^+ (square). Dashed lines are fits with an assumed location of the slipping plane at $1/5\kappa^{-1} + a + 2d_{\text{counter-ion}}$. Variables used in calculations were as follows: a = 2.55 nm, ε_r = 79 and z = 90.

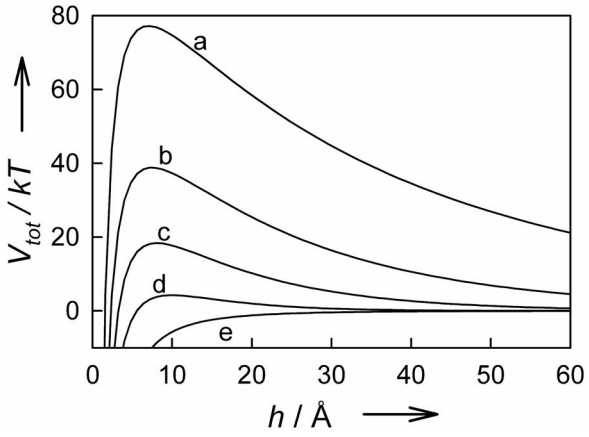

Figure 6. Interaction energy between two identical spheres at different salt concentrations: (a) 1 mM, (b) 10 mM, (c) 30 mM, (d) 90 mM and (e) > 1 M.

Table 1. Sizes of the counter-ions used[23].

	Na^+	TMA^+	TEA^+	TBA^+
r / Å	0.95	2.85	3.48	4.37

Table 2. Measured hydrodynamic sizes and zeta potentials before and after thiol exchange. Thiol exchange was done in two different TEAOH concentrations: 60 mM and 860 mM.

	Before	60 mM TEAOH	860 mM TEAOH
Diameter / nm	27.7	32.3	46
Zeta potential / mV	-43	-47	-58